2015

Effects Of Small Thundercloud Electrostatic Fields On The Ionospheric Density Profile

Mohammad A. Salem

Ningyu Liu

Hamid K. Rassoul

AGU PUBLICATIONS

Geophysical Research Letters

RESEARCH LETTER
10.1002/2015GL063268

Key Points:
- Thunderstorms can establish small electrostatic fields in the upper atmosphere
- Electron density can be reduced by 40% or increased by a factor of 6 due to thunderstorm fields
- Electron lifetime increases from a few milliseconds to tens of seconds in 40–80 km altitude range

Correspondence to:
M. A. Salem,
msalem2011@my.fit.edu

Citation:
Salem, M. A., N. Liu, and H. K. Rassoul (2015), Effects of small thundercloud electrostatic fields on the ionospheric density profile, *Geophys. Res. Lett.*, *42*, 1619–1625, doi:10.1002/2015GL063268.

Received 28 JAN 2015
Accepted 23 FEB 2015
Accepted article online 26 FEB 2015
Published online 25 MAR 2015

Effects of small thundercloud electrostatic fields on the ionospheric density profile

Mohammad A. Salem[1], Ningyu Liu[1], and Hamid K. Rassoul[1]

[1]Geospace Physics Laboratory, Department of Physics and Space Sciences, Florida Institute of Technology, Melbourne, Florida, USA

Abstract Small electrostatic fields of values not strong enough to activate electron impact ionization, attachment, and detachment processes can be established in the upper atmosphere by underlying thunderstorms. This paper investigates their effects on the ionospheric densities by using a simplified ion chemistry model. The modeling results indicate that under the steady state condition, the nighttime electron density profile can be reduced by up to ~40% or enhanced by a factor of up to ~6 because of the variation of the three-body electron attachment rate constant with the electric field.

1. Introduction

It is well known that electromagnetic fields produced by natural lightning activities at tropospheric altitudes can significantly affect the upper atmosphere. The ionospheric effects of lightning are directly evidenced by the production of transient luminous events (TLEs) with very short lifetimes, such as elves (<1 ms), halos (~2 ms), sprites (tens of milliseconds), and jets (hundreds of milliseconds) [*Liu*, 2014].

Thunderstorms and their lightning discharges can also modify the ionosphere on a longer time scale, during which TLEs may or may not occur. *Han and Cummer* [2010] used the ELF/VLF signals generated by distant lightning discharges and subsequently propagating in the Earth-ionosphere waveguide to probe the nighttime *D* region ionosphere (~75–90 km altitude) above an intervening thunderstorm. The ionospheric height changes over 2 months were extracted by fitting a series of simulated sferic spectra to the measured sferic spectrum. They found that the reference height of the ionosphere varies between 82.0 and 87.2 km, with a mean value of 84.9 km, on the time scales from minutes to hours. More recently, *Shao et al.* [2012] also analyzed the lightning-produced radio signals from a mesoscale thunderstorm to probe the nighttime *D* region above a small thunderstorm that was situated approximately midway between the mesoscale thunderstorm and a sensor. They compared the observed VLF/LF time waveforms to the simulation results of VLF/LF propagation to infer the most likely electron density profile. Over the lifetime of the small storm, the overhead *D* region electron density was observed to be reduced by several orders of magnitude below ~82 km altitude whereas increased at higher altitudes. The extent of the reduction was closely correlated with the lightning activity in the underlying thunderstorm and was mainly attributed to the electron attachment activated by relatively strong electric field in the lower ionosphere produced by the lightning discharges. However, according to several recent studies [e.g., *Liu*, 2012; *Luque and Gordillo-Vázquez*, 2012; *Neubert and Chanrion*, 2013], when the electric field is strong enough so that the electron impact ionization, attachment, and detachment processes become effective, the ionospheric electron density is not significantly reduced.

In this study, we investigate how small electrostatic fields (of values where the above mentioned processes are not effective) that may exist in the upper atmosphere during a thunderstorm affect the local steady state nighttime ionospheric density and examine whether significant reduction in the electron density can be achieved. The results from a simplified ion chemistry model indicate when the electric field varies from 0 to ~$0.4E_k$ (E_k is the conventional breakdown threshold field), the nighttime electron density profile can be reduced by ~40% or enhanced by a factor of ~6 because of the field-dependent rate constant of the three-body electron attachment.

2. The Steady State Nighttime Ion Chemistry Model of the Lower Ionosphere

2.1. Model Species and Reactions

Our study is conducted by using a simplified ion chemistry model described by *Liu* [2012]. The model is based on the one developed by *Lehtinen and Inan* [2007], which is in turn an improved version of the

Table 1. The Set of Chemical Reactions That Describe the Steady State Nighttime Ion Chemistry Model of the Lower Ionosphere

Reaction No.	Reactants	→	Products	Rate Constant ($m^{3(n-1)}\ s^{-1}$)[a]
		Ionization		
(R1)	$Q + M$	→	$e + M^+ + Q$	1×10^{-25}
		Three-Body Electron Attachment ($E/N = 0$ Td)		
(R2)	$e + M(O_2) + M$	→	$M^-(O_2^-) + M$	11.7×10^{-44}
		Three-Body Electron Attachment ($E/N > 0$ Td)		
(R3)	$e + M(O_2) + M$	→	$M^-(O_2^-) + M$	$f(\bar{\epsilon})$[b] $\equiv f(E/N)$[c]
		Recombination (Electron-Ion)		
(R4)	$e + M^+$	→	$M_{ac} + M_{ac}$	3×10^{-13}
(R5)	$e + M_x^+$	→	$M + M$	1×10^{-12}
		Recombination (Ion-Ion)		
(R6)	$M^- + M^+$	→	$M + M$	5×10^{-13}
(R7)	$M^- + M_x^+$	→	$M + M_x$	5×10^{-13}
(R8)	$M_x^- + M^+$	→	$M_x + M$	5×10^{-13}
(R9)	$M_x^- + M_x^+$	→	$M_x + M_x$	5×10^{-13}
(R10)	$M^- + M^+ + M$	→	$M + M + M$	5×10^{-37}
(R11)	$M^- + M_x^+ + M$	→	$M + M_x + M$	5×10^{-37}
(R12)	$M_x^- + M^+ + M$	→	$M_x + M + M$	5×10^{-37}
(R13)	$M_x^- + M_x^+ + M$	→	$M_x + M_x + M$	5×10^{-37}
		Ion Conversion		
(R14)	$M^+ + M + M$	→	$M_x^+ + M$	2×10^{-42}
(R15)	$M_x^+ + M$	→	$M^+ + M + M$	2×10^{-22}
(R16)	$M_x^+ + M_{ac}$	→	$M^+ + M$	1×10^{-16}
(R17)	$M^- + M + M$	→	$M_x^- + M$	1×10^{-43}
(R18)	$M_x^- + M_{ac}$	→	$M^- + M$	2×10^{-16}
		Electron Detachment		
(R19)	$M^- + M$	→	$e + M + M$	2×10^{-29}
(R20)	$M^- + M_{ac}$	→	$e + M + M_{ac}$	2.5×10^{-16}

[a]The rate constants are obtained from the work of *Liu* [2012]. The values of n are 2 and 3 for two-body and three-body reactions, respectively.
[b]$\bar{\epsilon}$ is the average electron energy in eV.
[c]E/N is the reduced electric field in Td.

Glukhov, Pasko, and Inan model proposed by *Glukhov et al.* [1992]. According to this model, the charged particles in the nighttime mesosphere and lower ionosphere can be grouped into five species: electrons (e), light negative ions (M^-), cluster negative ions (M_x^-), light positive ions (M^+), and cluster positive ions (M_x^+). The M^- ions include O^-, O_2^-, O_3^-, and O_4^-. The M_x^- ions include the stable CO_3^-, NO_3^-, HCO_3^-, and Cl^-. The M^+ ions comprise of mainly O_2^+ and NO^+. The M_x^+ ions are usually of the form $H^+(H_2O)_n$. Detailed discussion of the dominant ion species in the lower ionosphere can be found in *Liu* [2012] and *Brasseur and Solomon* [2005, pp. 553–575]. The neutral species can also be lumped into three groups: the neutral molecules (M) which mainly composed of O_2 and N_2; active neutrals (M_{ac}) such as nitrogen atoms, oxygen atoms, or excited states; and cluster molecules (M_x). Along with the aforementioned species, the model also includes cosmic ray particles (Q), as a steady source of ionization. The chemical reactions (ionization, attachment, recombination, ion conversion, and detachment) included in the model are listed in Table 1 together with their rate constants.

2.2. Model Equations

Under steady state conditions, the densities of the charged species can be found by solving a set of nonlinear equations:

$$\frac{dn_i}{dt} = 0 = S_i - L_i, \tag{1}$$

where n_i is the density of the ith charged species, and the local source (S_i) and the local loss (L_i) terms account for the change of the ith species density due to the chemical reactions shown in Table 1.

Along with the charge neutrality condition (the total density of negatively charged species equals to the total density of positively charged species), this system can be solved numerically by using a numerical solver such as the KINSOL module of the SUNDIALS software package developed by Lawrence Livermore National Laboratory (http://computation.llnl.gov/casc/sundials/main.html). A forward approach is employed in this study to calculate the densities of the charged species for a given ionization source profile. In contrast, a reverse approach was used in the work of *Liu* [2012] where the ionization source profile and the densities of other charged species are found from a prescribed electron density profile.

2.3. Three-Body Electron Attachment

Three-body electron attachment is the main process for electron loss when the electric field is not strong enough ($E \leq 0.4E_k$, where $E_k = 120$ Td) to activate electron impact ionization, attachment, and detachment processes. It is represented by the reaction (R3) in Table 1 whose rate constant (k_{3att}) depends on reduced

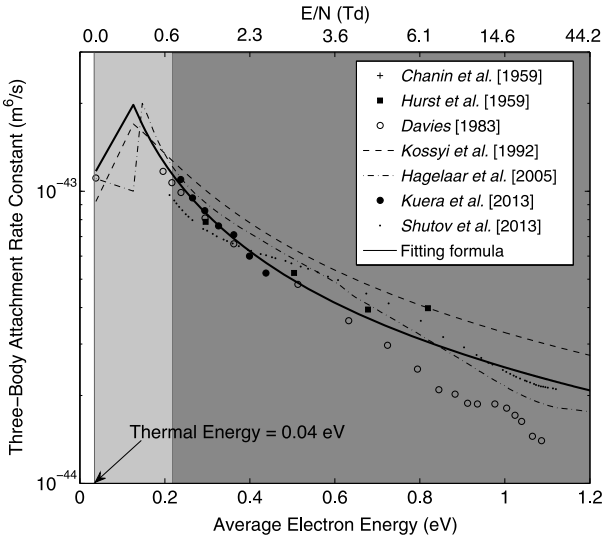

Figure 1. A comparison of the fitting formula (equation (2)) of the three-body rate constant as a function of average electron energy or as a function of E/N with experimental and theoretical studies available in the literature [e.g., *Chanin et al.*, 1959; *Hurst and Bortner*, 1959; *Davies*, 1983; *Kossyi et al.*, 1992; *Hagelaar and Pitchford*, 2005; *Kučera et al.*, 2013; *Shutov et al.*, 2013]. The dependence of $\bar{\epsilon}$ on E/N can be obtained from the work of *Moss et al.* [2006]. The light (dark) gray area represents the region where the electron density is expected to be reduced (increased), compared to its background profile, due to the variation of the three-body electron attachment rate (see section 3.2 for more details).

electric field (E/N, where E is the electric field and N is the atmospheric neutral density) and hence on average electron energy ($\bar{\epsilon}$). The dependence of $\bar{\epsilon}$ on E/N can be obtained from the work of *Moss et al.* [2006].

It should be noted that the three-body electron attachment process is already operative at thermal electron energies as shown in (R2). A review of the existing literature on the rate constant of this process [e.g., *Chanin et al.*, 1959; *Lennon and Mulcahy*, 1961; *Davies*, 1983; *Raizer*, 1991; *Kossyi et al.*, 1992; *Fridman and Kennedy*, 2004; *Kučera et al.*, 2013] leads us to conclude that in the absence of electric field, the average thermal k^0_{3att} from different sources is about 11.7×10^{-44} m^6/s.

There are no published investigations on the three-body electron attachment in air-like gas at very low values of E/N ($E/N < 0.6$ Td or $\bar{\epsilon} < 0.2$ eV). However, *Dutton et al.* [1963] suggested that the experimental data [e.g., *Hurst and Bortner*, 1959; *Chanin et al.*, 1962] for oxygen-nitrogen mixtures with low oxygen content can be used to compute k_{3att} for similar mixtures of different proportions. Hence, for air with 78% N_2 and 21% O_2

$$k_{3att} = 0.21^2(k_{O_2} + 3.7k_{N_2}),$$

where k_{O_2} and k_{N_2} are three-body rate constants for reaction (R3) in Table 1 when M represents O_2 and N_2, respectively. The values of k_{3att} at very low values of $\bar{\epsilon}$ are obtained by extrapolating k_{O_2} and k_{N_2} values given in *Hurst and Bortner* [1959], *Chanin et al.* [1962], *Kučera et al.* [2013], and *Shutov et al.* [2013]. When $\bar{\epsilon} \geq 0.13$ eV, the results from the previous studies indicated that the relationship between $\ln k_{3att}$ against $\ln \bar{\epsilon}$ is approximately linear. Finally, k_{3att} can be approximately fitted by the following piecewise formula:

$$k_{3att}(\bar{\epsilon}) = \begin{cases} (91.39\bar{\epsilon} + 8.27) \times 10^{-44} & \bar{\epsilon} < 0.13 \text{ eV} \\ 2.49 \times 10^{-44}(\bar{\epsilon})^{-1} & \bar{\epsilon} \geq 0.13 \text{ eV}. \end{cases} \quad (2)$$

A comparison between this formula with the experimental data and calculations available in the literature [e.g., *Hurst and Bortner*, 1959; *Chanin et al.*, 1962; *Davies*, 1983; *Kossyi et al.*, 1992; *Hagelaar and Pitchford*, 2005; *Kučera et al.*, 2013; *Shutov et al.*, 2013] is given in Figure 1. The fitting formula matches well with experimental data and theoretical calculations, so it is used for our study.

3. Results

3.1. Nighttime Densities of the Lower Ionosphere in the Absence of Electric Field

In the absence of electric field the total set of reactions listed in Table 1 except (R3) are taken into account when solving the set of equations (1). We first demonstrate our ion chemistry model is able to produce typical electron density profiles with different input profiles of ionization source. Two different nighttime ionization source profiles in the region from 40 to 90 km altitude are used: Q_1 is self-consistently calculated by the chemistry model when the electron density is prescribed as n_{e1} [*Liu*, 2012]; Q_2 is derived from the measured cosmic ray ionization rate profile [*Brasseur and Solomon*, 2005, p. 553] by using the rate constant of (R1). Two different and typical electron density profiles n_{e1} and n_{e2} are obtained as shown in Figure 2a.

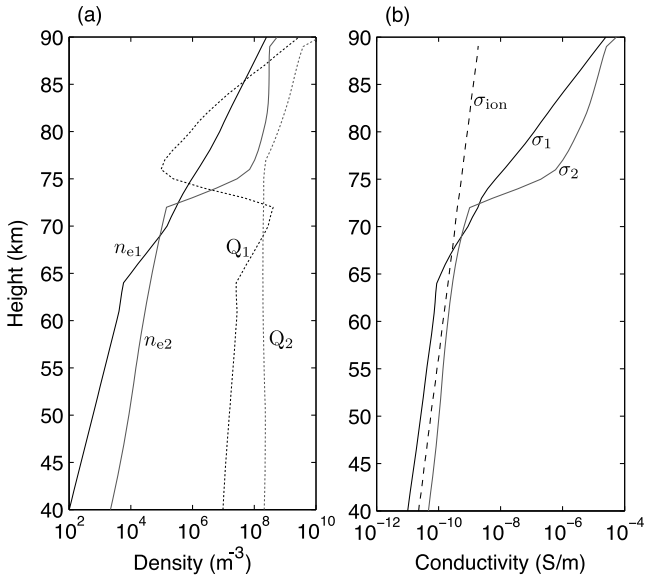

Figure 2. (a) Q_1 and Q_2 are the sources of nighttime ionization given in *Liu* [2012] and *Brasseur and Solomon* [2005, p. 553], respectively. The electron density profiles obtained from Q_1 and Q_2 are n_{e1} and n_{e2}, respectively, when $E/N = 0$ Td, and hence, $k_{3att} = 11.7 \times 10^{-44}$ m^6/s (see Figure 1). (b) The total conductivity profiles are σ_1 and σ_2 resulting from Q_1 and Q_2, respectively. The ion conductivity profile σ_{ion} is from measurements [*Holzworth et al.*, 1985].

Figure 2b shows the corresponding total conductivity profiles σ_1 and σ_2 obtained by using the mobility of the charged species from the work of *Liu* [2012], together with the measured ion conductivity profile reported by *Holzworth et al.* [1985]. It can be seen from Figure 2b that below 70 km altitude, where the conductivity is determined by the ion component [e.g., *Lehtinen and Inan*, 2007; *Liu*, 2012], they agree well and the measured σ_{ion} is bounded by σ_1 and σ_2. The deviation above 70 km is mainly because σ_{ion} does not include the electronic component, which is much larger than the ion component, as shown by the calculated results.

An ionospheric density profile often used to study thunderstorm effects [e.g., *Wait and Spies*, 1964; *Cheng and Cummer*, 2005; *Han and Cummer*, 2010] is described by the following formula:

$$n_e(z) = 1.43 \times 10^{13} \exp(-0.15h') \exp[(\beta - 0.15)(z - h')] \text{ m}^{-3}, \quad (3)$$

where h' in km and β in km^{-1} describe the reference altitude and the sharpness of the electron density profile, respectively. This equation has been used to measure the changes in the height of the lower ionosphere under the influence of thunderstorm lightning activities [*Cheng and Cummer*, 2005; *Han and Cummer*, 2010]. Therefore, we also use it to fit the modified ionosphere profile due to small thunderstorm electric fields in order to quantify the corresponding change in the reference height in the next section. Note that equation (3) can be fit to the n_{e1} profile in Figure 2a by using $h' = 85$ km and $\beta = 0.5$ km^{-1}.

3.2. Ionospheric Electron Density Changes Due to Small Electrostatic Fields

To quantify the effect of small electric fields on the ionospheric density, the calculation is repeated, but this time the reaction (R2) in Table 1 is replaced with (R3) whose rate constant is described by equation (2). We again consider both of the nighttime ionization source profiles Q_1 and Q_2, and the electron density changes under the influence of electric field ranging from 0 to 44.2 Td ($\sim 0.4E_k$) are examined at each specific altitude independently. As shown in Figure 3, the electron density profile is reduced (the light gray area) by ~40% or increased (the dark gray area) by a factor of ~6 below 80 km. By using equation (3) with β being fixed at 0.5 km^{-1}, and by only considering the relevant reflection altitude range of VLF waves, the best fit to the electron density profile at the largest decrease and at the largest increase is obtained when h' is 86.9 km and 82.3 km, respectively, which means the reference height of the disturbed ionosphere varies between those two values. The range of the reference height variation agrees well with the result obtained from the work of *Han and Cummer* [2010]. On the other hand, the maximum decrease and increase in the reference height for the electron density profile in Figure 3b is about 1.28 km and 0.5 km, respectively. Note also that there are no appreciable changes observed in regions above ~80 km altitude for both cases.

The changes in the electron density is attributed to the behavior of the k_{3att} described in Figure 1 where the rate constant increases linearly with the reduced electric field in the range of 0 to 0.1 Td while decreases exponentially from 0.1 Td to about $0.4E_k$. With this dependence, for electric field values in the range between 0 and 0.76 Td (the light gray area in Figures 1 and 3), the corresponding k_{3att} values exceed their ambient value, k^0_{3att}, and the resulting electron density is reduced with the maximum reduction occurring at 0.1 Td. In contrast, for electric field values greater than 0.76 Td (the dark gray area in Figures 1 and 3), the corresponding k_{3att} values are lower than k^0_{3att}, and so the electron density is increased and the maximum

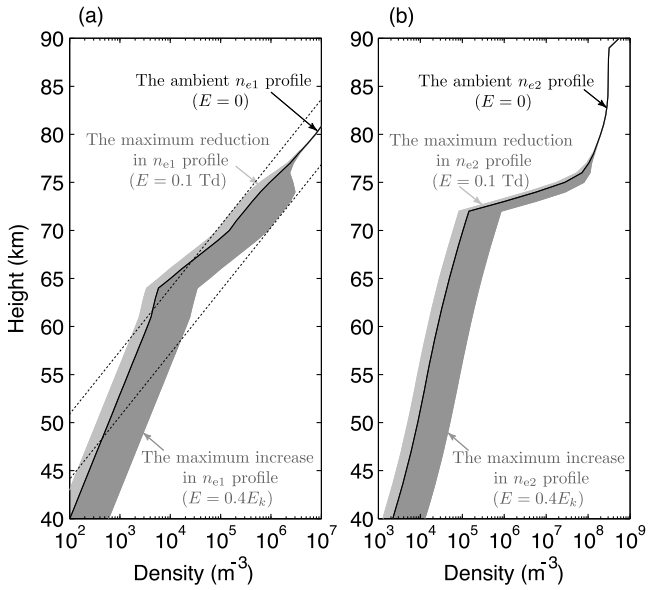

Figure 3. The range of the corresponding electron density variations for the nighttime ionization sources: (a) Q_1 and (b) Q_2, when the electric field varies from 0 Td to 44.2 Td ($\sim 0.4E_k$) at each specific altitude independently. The light (dark) gray area represents the region where the electron density is reduced (increased) when the electric field varies from 0 Td to 0.76 Td (0.76 Td to $\sim 0.4E_k$). The upper and lower dotted lines in Figure 3a are the electron density profiles described with equation (3) with $\beta = 0.5$ km^{-1}, $h' = 86.9$ and 82.3 km, respectively.

increase happens at $\sim 0.4E_k$. It should be noted that the maximum rate constant of the three-body attachment from all the studies shown in Figure 1 is accounted for when using equation (2). It is therefore expected that the maximum reduction in electron density obtained from our calculations is no less than what is obtained from using the results from a particular study. However, the minimum rate constant from those studies is about a factor of 1.5 smaller than the minimum value given by equation (2) in the electric field range of interest. Additional calculations indicate that the electron density may be further increased by a factor of 2. Finally, the aforementioned results may change if there are other electron production or loss processes whose rate constants depend sensitively on the electric field in the range considered here.

4. Discussion

4.1. Small Electrostatic Fields Above Thunderclouds

Small electrostatic fields in the altitude range of interest to our study can be established by underlying thunderclouds. Under steady state condition, the conducting current density (J_{cond}) above thunderclouds is equal to the charging current density due to convection (J_{conv}) inside thunderclouds. Assuming a simple planar geometry, the magnitude of the vertical component of the electric field (E_z) at a specific altitude above a thundercloud is given by Ohm's law:

$$E_z = \frac{J_{\text{cond}}}{\sigma_z} = \frac{J_{\text{conv}}}{\sigma_z}, \tag{4}$$

where σ_z is the conductivity at that altitude. J_{conv} inside thunderclouds is about 10^{-8} A/m^2 [*Riousset et al.*, 2010]. According to the above equation, the electric field at 69 km altitude, for example, where the conductivity is about 5.5×10^{-10} S/m (see Figure 2), equals to 18.2 V/m ($\sim$10 Td). Due to the relatively large conductivity values above 80 km, the values of electric field are very small (i.e., close to its ambient value) and the changes in electron density profiles in this region are negligible, as shown by Figure 3. In addition, small, long-lasting *QE* field of tens of mV/m can be established at high altitudes by relatively weak but frequent lightning discharges [*Inan et al.*, 1996].

4.2. Lifetimes of the Ion Species

The lifetime of the *i*th species at a specific altitude (τ_i) can be estimated by dividing the species densities obtained in section 3 (not shown in Figure 2 for species other than electrons but can be found in *Liu* [2012]) by the rate of loss of that species at the same altitude. Figure 4a shows the electron lifetime against the reactions that are responsible for electron loss ((R3)–(R5)) and also the total electron lifetime when $k_{3\text{att}}$ changes from its minimum value to its maximum at each specific altitude. The total lifetimes of the other charged species over the same range of $k_{3\text{att}}$ values are also shown in Figure 4b with the lifetime-dominant reaction is given below each species. It should be noted that the lifetimes of all the species other than electrons do not change when the electric field changes over the corresponding range. On the other hand, it can be seen that the total electron lifetime is dominated by the fastest reaction, (R3), which is independent of any charged species. The lifetime of electrons, which ranges from a few milliseconds at 40 km altitude up to 10–100 s at 80 km altitude, is in good agreement with the recovery time of very low frequency signals

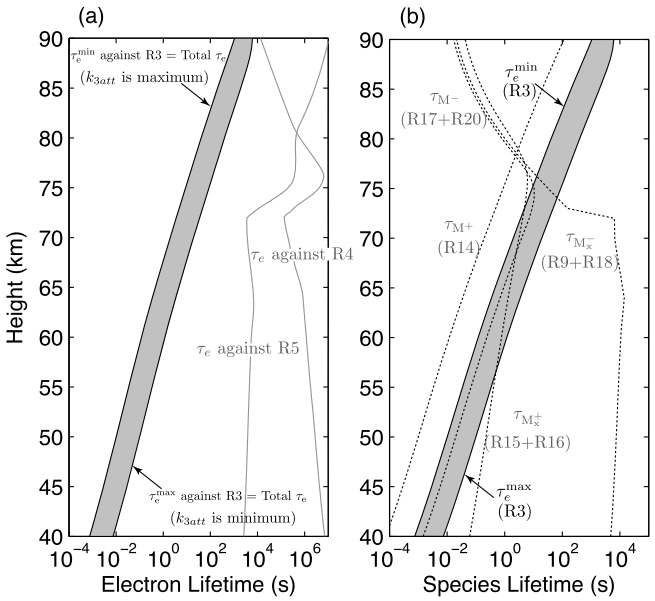

Figure 4. (a) The lifetime of electrons (τ_e) when k_{3att} changes from its minimum value to its maximum value at each altitude. (b) The lifetime of all species (τ_i, where $i = e$, M^-, M_x^-, M^+, and M_x^+) over the same range of k_{3att} at each altitude. The reaction numbers surrounded by parentheses below each species represent the dominant reaction in calculation of the lifetime of that species. The gray regions represent the limits of the total electrons lifetime.

in the work of *Inan et al.* [1996]. This lifetime is smaller than the life span of thunderstorms, which varies from less than an hour for single-cell thunderstorms to several hours for multicell thunderstorms [e.g., *Reddy et al.*, 2014]. Therefore, steady state electron density can be fulfilled above thunderclouds.

According to the results of the present study, the maximum reduction in electron density profile under the effect of small electrostatic fields in the range mentioned above is only about 40%. Even if the field exceeds this range to the extent that the two-body attachment cannot be ignored, it is still difficult to reduce the electron density because of an electron detachment process [*Liu*, 2012]. On the other hand, our results are consistent with the finding of *Han and Cummer* [2010] that the nightly variations in the electron density over 2 months of observations are dominated by a descending ionosphere.

Given the above discussion, the observed significant increase in the ionosphere height reported by *Shao et al.* [2012] may be attributed to the following two scenarios. First, if somehow the ambient electric field has a specific value rather than zero and it is decreased to the value where k_{3att} peaks (see Figure 1), the electron density will decrease significantly, but less than a factor of 10 according to the results presented in the previous section. The extent of reduction in this case will depend on the initial value of the electric field. Secondly, the electron mobility (μ_e) also reduces significantly when electric field increases [*Davies*, 1983]. Therefore, the measured increase in the ionospheric height may be due to the reduction in the conductivity ($\sigma_e = en_e\mu_e$) rather than the electron density.

Acknowledgments

Table 1 lists the reactions of our ionosphere chemistry model and their corresponding rate constants. The MSIS atmosphere model used in our study for the neutral density profiles is available at http://omniweb.gsfc.nasa.gov/vitmo/msis_vitmo.html. This research was supported in part by NSF grant AGS-0955379.

The Editor thanks Robert Marshall and an anonymous reviewer for their assistance in evaluating this paper.

References

Brasseur, G. P., and S. Solomon (2005), *Aeronomy of the Middle Atmosphere: Chemistry and Physics of the Stratosphere and Mesosphere, Atmospheric and Oceanographic Sciences Library* third revised and enlarged ed., vol. 32, Springer, Netherlands.

Chanin, L. M., A. V. Phelps, and M. A. Biondi (1959), Measurement of the attachment of slow electrons in oxygen, *Phys. Rev. Lett.*, *2*, 344–346, doi:10.1103/PhysRevLett.2.344.

Chanin, L. M., A. V. Phelps, and M. A. Biondi (1962), Measurements of the attachment of low-energy electrons to oxygen molecules, *Phys. Rev.*, *128*, 219–230, doi:10.1103/PhysRev.128.219.

Cheng, Z., and S. A. Cummer (2005), Broadband VLF measurements of lightning-induced ionospheric perturbations, *Geophys. Res. Lett.*, *32*, L08804, doi:10.1029/2004GL022187.

Davies, D. K. (1983), Measurements of swarm parameters in dry air, theoretical notes, *Tech. Rep., Note 346*, Westinghouse R&D Center, Pittsburg.

Dutton, J., F. Harris, and F. L. Jones (1963), The influence of the three-body process of electron attachment on the growth of ionization in air at high pressure, *Proc. Phys. Soc.*, *82*(4), 581.

Fridman, A., and L. A. Kennedy (2004), *Plasma Physics and Engineering*, CRC Press, New York.

Glukhov, V. S., V. P. Pasko, and U. S. Inan (1992), Relaxation of transient lower ionospheric disturbances caused by lightning-whistler-induced electron-precipitation bursts, *J. Geophys. Res.*, *97*(A11), 16,971–16,979, doi:10.1029/92JA01596.

Hagelaar, G. J. M., and L. C. Pitchford (2005), Solving the Boltzmann equation to obtain electron transport coefficients and rate coefficients for fluid models, *Plasma Sources Sci. Technol.*, *14*, 722–733, doi:10.1088/0963-0252/14/4/011.

Han, F., and S. A. Cummer (2010), Midlatitude nighttime D region ionosphere variability on hourly to monthly time scales, *J. Geophys. Res.*, *115*, A09323, doi:10.1029/2010JA015437.

Holzworth, R. H., M. C. Kelley, C. L. Siefring, L. C. Hale, and J. T. Mitchell (1985), Electrical measurements in the atmosphere and the ionosphere over an active thunderstorm: 2. Direct current electric fields and conductivity, *J. Geophys. Res.*, *90*, 9824–9830.

Hurst, G. S., and T. E. Bortner (1959), Attachment of low-energy electrons in mixtures containing oxygen, *Phys. Rev.*, *114*, 116–120, doi:10.1103/PhysRev.114.116.

Inan, U. S., V. P. Pasko, and T. F. Bell (1996), Sustained heating of the ionosphere above thunderstorms as evidenced in "early/fast" VLF events, *Geophys. Res. Lett.*, *23*(10), 1067–1070, doi:10.1029/96GL01360.

Kossyi, I. A., A. Y. Kostinsky, A. A. Matveyev, and V. P. Silakov (1992), Kinetic scheme of the non-equilibrium discharge in nitrogen-oxygen mixtures, *Plasma Sources Sci. Technol.*, *1*(3), 207–220.

Kučera, M., M. Stano, J. Wnorowska, W. Barszczewska, D. Loffhagen, and Š. Matejčík (2013), Electron attachment to oxygen in nitrogen buffer gas at atmospheric pressure, *Eur. Phys. J. D*, *67*(11), 234, doi:10.1140/epjd/e2013-40401-2.

Lehtinen, N. G., and U. S. Inan (2007), Possible persistent ionization caused by giant blue jets, *Geophys. Res. Lett.*, *34*, L08804, doi:10.1029/2006GL029051.

Lennon, J. J., and M. J. Mulcahy (1961), Microwave measurement of attachment in oxygen-nitrogen mixtures, *Proc. Phys. Soc.*, *78*(6), 1543–1545.

Liu, N. Y. (2012), Multiple ion species fluid modeling of sprite halos and the role of electron detachment of O^- in their dynamics, *J. Geophys. Res.*, *117*, A03308, doi:10.1029/2011JA017062.

Liu, N. Y. (2014), Upper atmospheric electrical discharges, in *The Lightning Flash*, 2nd ed., edited by V. Cooray, pp. 725–786, The Institution of Engineering and Technology, London.

Luque, A., and F. Gordillo-Vázquez (2012), Mesospheric electric breakdown and delayed sprite ignition caused by electron detachment, *Nat. Geosci.*, *5*(1), 22–25, doi:10.1038/NGEO1314.

Moss, G. D., V. P. Pasko, N. Liu, and G. Veronis (2006), Monte Carlo model for analysis of thermal runaway electrons in streamer tips in transient luminous events and streamer zones of lightning leaders, *J. Geophys. Res.*, *111*, A02307, doi:10.1029/2005JA011350.

Neubert, T., and O. Chanrion (2013), On the electric breakdown field of the mesosphere and the influence of electron detachment, *Geophys. Res. Lett.*, *40*, 2373–2377, doi:10.1002/grl.50433.

Raizer, Y. P. (1991), *Gas Discharge Physics*, Springer, New York.

Reddy, C., P. Anisha, and L. Prasad (2014), Detection of thunderstorms using data mining and image processing, in *2014 Fifth International Conference on the Applications of Digital Information and Web Technologies (ICADIWT)*, pp. 226–231, IEEE, doi:10.1109/ICADIWT.2014.6814672.

Riousset, J. A., V. P. Pasko, P. R. Krehbiel, W. Rison, and M. A. Stanley (2010), Modeling of thundercloud screening charges: Implications for blue and gigantic jets, *J. Geophys. Res.*, *115*, A00E10, doi:10.1029/2009JA014286.

Shao, X.-M., E. H. Lay, and A. R. Jacobson (2012), Reduction of electron density in the night-time lower ionosphere in response to a thunderstorm, *Nat. Geosci.*, *6*(1), 29–33, doi:10.1038/ngeo1668.

Shutov, A. V., I. V. Smetanin, A. A. Ionin, A. O. Levchenko, L. V. Seleznev, D. V. Sinitsyn, N. N. Ustinovskii, and V. D. Zvorykin (2013), Direct measurement of the characteristic three-body electron attachment time in the atmospheric air in direct current electric field, *Appl. Phys. Lett.*, *103*(3), 034106, doi:10.1063/1.4813601.

Wait, J. R., and K. P. Spies (1964), Characteristics of the Earth-ionosphere waveguide for VLF radio waves, *Tech. Note 300*, Natl. Bur. of Stand., Boulder, Colo.